

Spin Hamiltonian, Competing Small Energy Scales and Incommensurate Long Range Order in the Highly Frustrated $\text{Gd}_3\text{Ga}_5\text{O}_{12}$ Garnet Antiferromagnet

Taras Yavors'kii,¹ Matthew Enjalran,² and Michel J.P. Gingras^{1,3}

¹ *Department of Physics and Astronomy, University of Waterloo, Waterloo, Ontario, N2L 3G1, Canada*

² *Department of Physics, Southern Connecticut State University, New Haven, CT 06515, USA*

³ *Department of Physics and Astronomy, University of Canterbury, Private Bag 4800, Christchurch, New Zealand*

(Dated: September 21, 2018)

Despite the availability of a spin Hamiltonian for the $\text{Gd}_3\text{Ga}_5\text{O}_{12}$ garnet (GGG) for over twenty five years, there has so far been little theoretical insight regarding the many unusual low temperature properties of GGG. Here we investigate GGG in zero magnetic field using mean-field theory. We reproduce the spin liquid-like correlations and, most importantly, explain the positions of the sharp peaks seen in powder neutron diffraction experiments. We show that it is crucial to treat accurately the long-range nature of the magnetic dipolar interactions to allow for a determination of the small exchange energy scales involved in the selection of the experimental ordering wave vector. Our results show that the incommensurate order in GGG is classical in nature, intrinsic to the microscopic spin Hamiltonian and not caused by weak disorder.

The diversity of empirical data collected over the past fifteen years has demonstrated that geometrically frustrated triangular and tetrahedral arrangements of antiferromagnetically coupled spins are highly partial towards the realization of exotic correlated phases in magnetic materials [1, 2, 3]. The reason for the rich and typically material specific properties of frustrated magnets is understood. It stems from their sensitivity to perturbations beyond the frustrating nearest-neighbor antiferromagnetic (AFM) exchange which, on its own, leads to a macroscopic number of exactly degenerate and competing, hence fragile, classical ground states. In this paper we show, through a careful theoretical analysis of neutron scattering experiments, that the extensively studied $\text{Gd}_3\text{Ga}_5\text{O}_{12}$ garnet (GGG) is precisely such a system, though evidence for this fact emerges from a perspective on the problem that has heretofore escaped scrutiny.

GGG displays a gamut of complex and interesting low temperature magnetic phenomena. In zero magnetic field, the behavior of GGG is uniquely rich. The nonlinear magnetic susceptibility χ_3 peaks at $T_g \sim 180$ mK [4], indicating a spin glass transition [5]. However, muon spin relaxation [6, 7] and Mössbauer spectroscopy [8] find persistent spin dynamics down to $T \ll T_g$. Meanwhile, powder neutron scattering data [9, 10] indicate that GGG is on the verge of developing true incommensurate long-range magnetic order with a correlation length ($\xi \approx 100$ Å) extending over 8 cubic unit cells below 140 mK.

A Hamiltonian \mathcal{H} describing GGG, that we shall explicitly define below, has long been available [11]. It assumes classical Gd^{3+} spins, is parameterized as a sum of empirical exchange contributions up to third nearest-neighbors as well as a magnetic dipolar contribution, and ignores potentially important quantum fluctuations or disorder inherent to GGG [4]. Previous numerical studies based on \mathcal{H} have been unable to provide a quantitative explanation for the bulk [4] and dynamical [6, 7, 8] properties of GGG or the incommensurate spin-spin correla-

tions that develop below 200 mK [9, 10]. This could be interpreted as evidence that exotic mechanisms involving either quantum fluctuations or disorder effects are at play in GGG. For example, it has been suggested that disorder, such as Gd^{3+} on Ga^{3+} sites, is responsible for nucleating regions with the spin order observed in neutron scattering in zero magnetic field [9, 10].

In this letter we address the adequacy of the Hamiltonian \mathcal{H} of Ref. 11 to explain the low temperature properties of GGG. It has been demonstrated [9, 12] that \mathcal{H} with only a nearest-neighbor exchange interaction can describe liquid-like spin correlations [9, 10]. We show below that \mathcal{H} can also describe well the incommensurate spin-spin correlations and that there is no obvious reason to extend \mathcal{H} . Rather, it is the correct procedure to treat its many competing small energy scales, in particular the long range dipolar interactions, and the unusually precise specification of weak second and third nearest-neighbor exchange couplings, that are foremost needed, and that have been missed so far.

In order to correctly parameterize \mathcal{H} and the resulting spin correlations we rely on neutron scattering experiments [9, 10], which are the most direct and unambiguous probe of magnetic correlations. Our basic hypothesis is that conventional criticality controls the development of the sharp peaks observed in neutron experiments [9, 10], and that, as in conventional magnets, a mean-field theory (MFT) treatment of the pertinent Hamiltonian should be able to capture the Gaussian regime in the approach to criticality. Our finding of a unique ordering wave vector \mathbf{q}_{ord} shows that GGG, unlike the AFM nearest-neighbor Heisenberg pyrochlore, is not pathological and is amenable to such a soft-mode determination and calculation of the neutron scattering intensity profile. We show that GGG is very similar to the now well understood dipolar spin ice materials [13, 14], where a MFT that takes into account the long-range nature of the dipolar interaction [13] (i) identifies the correct ordering wave

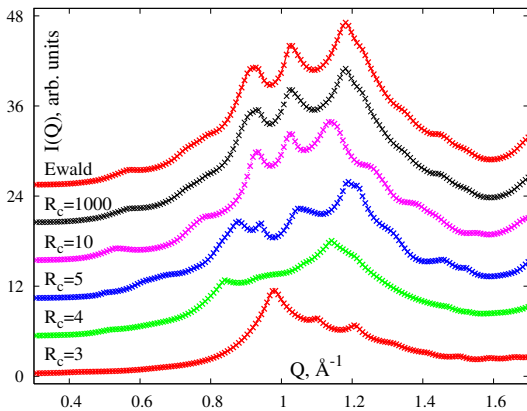


FIG. 1: MFT $I(Q)$ of GGG with $J_2 = -0.003$ K, $J_3 = 0.010$ K [11] and $\tau = 10^{-4}$ for $R_c = 3, 4, 5, 10, 1000$. The $R_c = \infty$ profile is obtained using the Ewald method. The profiles are uniformly shifted to emphasize their strong dependence on R_c for small values, as well as their saturation to a well defined limit at large R_c .

vector [14], and (ii) correctly predicts the symmetry of the scattering close to the critical temperature.

We examine the spin correlations in GGG by calculating the powder neutron scattering intensity $I(Q)$ and comparing it with experimental data [9]. The scattering \mathbf{q} -vector-dependent intensity is given by $I(\mathbf{q}) = (F(|\mathbf{q}|)^2/N) \sum_{ij} \langle \mathbf{S}_i^\perp \cdot \mathbf{S}_j^\perp \rangle e^{i\mathbf{q} \cdot \mathbf{r}_{ij}}$, obtained for the model Hamiltonian [11] $\mathcal{H} = \mathcal{H}_e + \mathcal{H}_{\text{dip}}$ with $\mathcal{H}_e = \sum_{i>j} \left\{ \sum_{n=1}^3 J_n \delta_{r_{ij}, r_n} \mathbf{S}_i \cdot \mathbf{S}_j \right\}$ and $\mathcal{H}_{\text{dip}} = \sum_{i>j} [D(r_1/r_{ij})^3] [\mathbf{S}_i \cdot \mathbf{S}_j - 3(\mathbf{S}_i \cdot \hat{r}_{ij})(\mathbf{S}_j \cdot \hat{r}_{ij})]$. Labels i and j span the N sites of a garnet lattice (c.f. Fig. 2 in Ref. [11]), r_{ij} and \hat{r}_{ij} are the length and direction of the vector separation between them, and r_n enumerate distances between the sites starting from the nearest neighbors. The size of the GGG conventional cubic unit cell is $a = 12.349$ Å [9]. The isotropic vectors \mathbf{S}_i have length $\sqrt{S(S+1)}$ to classically approximate the $S = 7/2$ Gd³⁺ spins. \mathbf{S}_i^\perp are the spin components perpendicular to \mathbf{q} , $F(|\mathbf{q}|)$ is the Gd³⁺ magnetic form-factor [15], and $\langle \dots \rangle$ denotes a thermal average. The spin couplings in \mathcal{H} include dipolar interactions \mathcal{H}_{dip} of strength D , cut-off at a distance R_c , and exchange interactions of empirical strength J_n , $n \leq 3$. We show below that R_c must be set to the true long-range limit $R_c = \infty$ in order to obtain physically meaningful results. Throughout the paper, we keep $D = 0.0457$ K [12] and the nearest-neighbor exchange $J_1 = 0.107$ K [11] fixed. However, because of the large uncertainties on J_2 and J_3 estimated from high-temperature analysis ($-0.015 \leq J_2 \leq 0.009$ K, $-0.035 \leq J_3 \leq 0.100$ K) [11], and the unreliability of the Monte Carlo procedure [11] to refine them because of poor statistics (see also discussion in Ref. [10]), we consider these as free parameters to be adjusted by fitting the experimental $I(Q)$ [9].

We use a Gaussian MFT [16] to obtain the soft modes and calculate $I(Q)$ of the model \mathcal{H} . Using a self-adaptive \mathbf{q} -grid, we can calculate $I(\mathbf{q})$ (in the thermodynamic limit) at an arbitrary positive dimensionless temperature $\tau = T/T_c^{\text{MFT}} - 1$, where $T_c^{\text{MFT}} \approx 2$ K and depends on J_2 and J_3 . Due to the $\log|\tau|$ growth of the powder MFT Bragg peak intensities, as opposed to the $1/\tau$ growth of the \mathbf{q} -dependent intensities, τ must be set rather small in order to work with the experimental profiles in the critical regime (cf. Fig. 4). We consider a finite \mathbf{q} -space grid with 32^3 points in the first Brillouin zone, and construct a three dimensional cubic interpolation scheme to separately evaluate the numerator and the denominator of the MFT $I(\mathbf{q})$ (cf. Eq. A37 in Ref. 16). For $\mathbf{q} \approx \mathbf{q}_{\text{ord}} + \mathbf{G}$, where Bragg peaks occur (\mathbf{G} is a FCC reciprocal lattice vector), we back up the interpolation by calculating $I(\mathbf{q})$ exactly [16]. This ensures \mathbf{q} -grid size independent results [16]. $I(Q)$ is computed by spherically averaging $I(\mathbf{q})$ numerically.

We find that \mathcal{H} with dipolar interactions and exchange interactions beyond nearest-neighbor possesses a unique \mathbf{q}_{ord} . Our numerical study suggests that the soft mode selection in the full \mathcal{H} is highly sensitive to the values of J_2 and J_3 . This finding is in general agreement with results from Monte Carlo simulations of GGG [9, 10] (see also Ref. [11] for a comment on the sensitivity of the GGG specific heat on J_3). However, our crucial new observation is that \mathbf{q}_{ord} is also very sensitive to an ad-hoc choice of the cut-off distance R_c in \mathcal{H}_{dip} . We demonstrate this by plotting in Fig. 1 $I(Q)$ for various R_c for $J_2 = -0.003$ K and $J_3 = 0.010$ K (values from [11]). For $R_c \lesssim O(10^2)$, not only is \mathbf{q}_{ord} a non-monotonous function of R_c , as the positions of the peaks indicate, but so is the unit cell magnetic form factor, as is evident from the significant changes in the overall shape of the diffuse scattering patterns near criticality ($\tau \ll 1$). Fig. 1 demonstrates that \mathcal{H} with different low R_c gives completely different spin-spin correlations in the critical regime. Only for rather large cut-offs does \mathbf{q}_{ord} become insensitive to R_c , approaching the $R_c = \infty$ limit only when $R_c \gtrsim 10^3$. Figure 1 suggests that it is essential to set R_c to its true $R_c = \infty$ limit to avoid inducing spurious ordered phases by treating the lattice sum in \mathcal{H}_{dip} by a short cut-off method, as was done previously [9, 10, 11, 12, 17]. We henceforth acknowledge this and implement the Ewald method [16] to process \mathcal{H}_{dip} with $R_c = \infty$.

The scattering profiles in Fig. 1 and the \mathbf{q} positions of the sharp peaks, even in the $R_c = \infty$ limit, are incompatible with the experimental data [9] (cf. Fig. 4, upper panel). However, the uncertainty in previously estimated values of J_2 and J_3 [11] allows fine-tuning them in order to obtain a better match with the low temperature data [9]. To proceed, we are guided by the general understanding of disordered systems near the critical boundary between long-range ordered and spin glass phases [5]. Specifically, we make the reasonable assumption that,

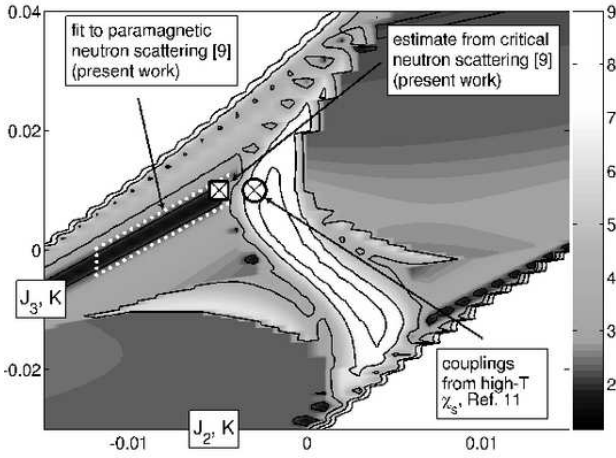


FIG. 2: The optimization neutron-scattering penalty function, \mathcal{P} , in the $J_2 - J_3$ plane behaves discontinuously and shows minima in the black domains. Only for the couplings demarcated by a dotted trapezoid does the theoretical scattering profile reconstitute both the location of the sharp peaks and the overall shape of the broad and diffuse experimental scattering [9, 10]. The circle corresponds to the values of J_2 and J_3 suggested in Ref. 11. The upper-left and bottom-right white regions correspond to different $\mathbf{q}_{\text{ord}} = 0$ structures.

given the sizeable and saturated $\xi \sim 100 \text{ \AA}$ correlated regions below 140 mK [9], the weak disorder in GGG freezes-in the \mathbf{q} -dependence of quasi-critical incommensurate correlated regions as T_g is crossed upon cooling. We therefore use a two-step fitting procedure to determine J_2 and J_3 . First, we establish whether the model \mathcal{H} allows for a \mathbf{q}_{ord} compatible with the experiment. Second, we examine whether the model with a given $\{J_2, J_3\}$ set is able to reproduce the overall structure of correlations both in the paramagnetic and “frozen-in critical” regimes [9].

We find that \mathbf{q}_{ord} for $R_c = \infty$ belongs to the (hhl) reciprocal plane, with its location within the plane highly dependent on J_2 and J_3 . To determine the optimum J_2 and J_3 , we generate a sequence of data points $\{\tilde{Q}\} \equiv |\mathbf{q}_{\text{ord}}(J_2, J_3) + \mathbf{G}|$, and then match these points to the experimental sequence of sharp peaks in powder GGG data [9]. To do so, we introduce a penalty function, $\mathcal{P}(J_2, J_3)$, that provides a measure of mismatch between the first three clearly discernible and strongest experimental peaks at $Q_1^* = 0.64 \text{ \AA}^{-1}$, $Q_2^* = 0.85 \text{ \AA}^{-1}$ and $Q_3^* = 1.07 \text{ \AA}^{-1}$ of Ref. 9 (see 43mK experimental data in top panel of Fig. 4) and the closest theoretically determined peaks: $\mathcal{P} = 100 \times \max_{i=1,2,3} \Delta Q_i$, where $\Delta Q_i = \min_{\tilde{Q} \in \{\tilde{Q}\}} |\tilde{Q} - Q_i^*|$ with the numerical factor 100 chosen to set the scale, $\mathcal{P} \equiv 1$, for a maximum mismatch of 0.01 \AA^{-1} . A map of \mathcal{P} in the $J_2 - J_3$ plane is shown in Fig. 2. A good match between theory and experiment is denoted in black. The discrepancy between experiment and theory increases as the gradation of gray varies from black to white.

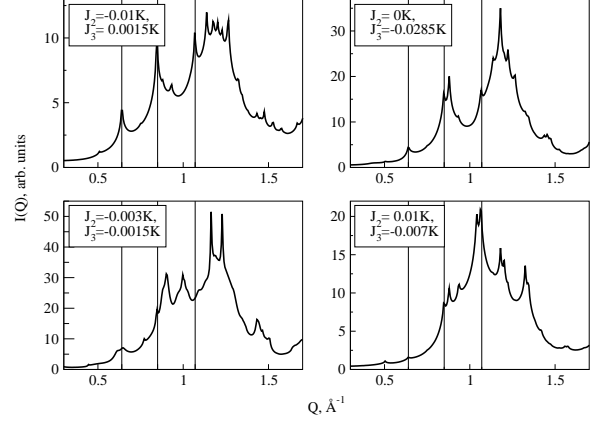


FIG. 3: Scattering profile for regions of the $J_2 - J_3$ plane where the positions Q_i of the sharp peaks have been optimized; $\tau = 1.6 \times 10^{-6}$. Upper left and bottom right panels represent correspondingly located black domains in Fig. 2. The other two panels represent small domains in the central and bottom-left part of Fig. 2. The overall shape of $I(Q)$ varies significantly, but all the profiles display sharp peaks agreeing with the experiment (shown by vertical lines).

Figure 2 shows that even small (at the $\approx 1\%$ level of J_1) changes in J_2 and J_3 show up as large changes in the ordering wave vector and, correspondingly, in \mathcal{P} too. There exist only relatively small domains (shown in black) that minimize \mathcal{P} . It turns out, however, that for each of these domains, the overall shape of the MFT powder scattering profile changes noticeably even though \mathbf{q}_{ord} remains almost constant at the value of $2\pi/a [0.29, 0.29, 0]$. Similarly to the standard experimental procedure to analyze powder neutron scattering data, once \mathbf{q}_{ord} is determined, one needs to solve for the magnetic structure. The sensitivity of the unit cell magnetic form factor to $\{J_2, J_3\}$ leads to a significant *qualitative* change in the diffuse scattering pattern near criticality, hence offering a second optimization channel for the determination of $\{J_2, J_3\}$.

Figure 3 shows the dependence of the theoretical $I(Q)$ on $\{J_2, J_3\}$ within the black domains of Fig. 2. A comparison of such theoretical profiles with the experimental one reveals that *only* in the upper left black domain are the theoretical and experimental profiles similar; a strong discrepancy in other domains allows us to exclude them from further consideration. Within the upper left domain, the match is visually better for rightmost values of J_2 with the restriction that its value cannot cross the domain boundary at -0.004K .

We support and further refine the above analysis by fitting the MFT scattering profiles to the experimental $I(Q)$ in the paramagnetic regime. For each value of J_2 and J_3 we consider a χ^2 -type penalty function for the overall shape of $I(Q)$, which is adjusted by parameters responsible for a uniform and linear in $|Q|$ background terms, as well as by the overall scale factor. With τ as a free fitting parameter, we do the fits in the interval

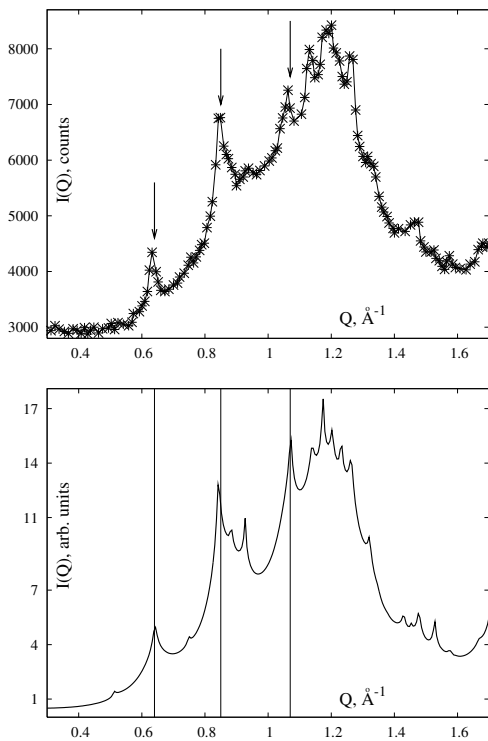


FIG. 4: Positions of the first three strongest peaks of the experimental scattering profile (pointed to by arrows in the upper panel) as well as the overall shape of scattering profile are used as criteria for the optimization procedure in the $J_2 - J_3$ plane. The resulting mean-field theory profile at dimensionless temperature $\tau = 1.6 \times 10^{-6}$ (lower panel) compares well with the experimental one. The positions of three experimental peaks are denoted by vertical lines. The experimental scattering profile has been obtained by digitizing Fig. 2 of Ref. 9. The theoretical profile is shown for $J_2 = -0.005K$, $J_3 = 0.010K$, denoted by a box in Fig. 2.

$Q = 0.26 - 1.57\text{\AA}^{-1}$ which allows for the complete shape determination of the first experimental broad diffusive scattering peak at 1.05\AA^{-1} without a $|Q|^2$ background correction. Most importantly, an analysis of the (paramagnetic) data at 175 mK [9] allows us to confirm the outcome of the analysis of the critical data at 43 mK and reject all but the aforementioned upper left domain of Fig. 2. Within that domain the data impose conservative error bars on J_2 : $-0.012\text{ K} \leq J_2 \leq -0.004\text{ K}$, with limits on J_3 set by that same domain, i.e. $-0.003\text{ K} \leq J_3 \leq 0.012\text{ K}$, see Fig. 2.

The MFT $I(Q)$ with the optimized J_n values captures the features of the experimental $I(Q)$ well (see bottom panel of Fig. 4). The optimization procedure to match the three strongest experimental peaks leads to a theoretical sequence of peaks that can be identified on the experimental profile as rather well-distinguished peaks and cusps. The match (Fig. 4) between MFT and experimental $I(Q)$ suggests post-factum that the \mathbf{q}_{ord} dependence of the correlations can be described by MFT.

To conclude, we have found that, as in spin ices [1, 13, 14], an ad-hoc R_c cut-off of the dipolar interactions at less than a few hundred nearest-neighbor distances leads to spurious long-range ordered phases. Only a proper treatment of an infinite R_c allows one to get a handle on the very small exchange interactions beyond nearest neighbors which dictate the incommensurate ordering wave vector \mathbf{q}_{ord} . With a reasonably well parameterized Hamiltonian now in hand, further theoretical studies to explore the origins of the complex phenomena displayed by GGG in zero and nonzero magnetic field may now be possible. Perhaps most importantly, we have identified the likely reciprocal plane that contains \mathbf{q}_{ord} , with $\mathbf{q}_{\text{ord}} \approx 2\pi/a [0.29, 0.29, 0]$. With this prediction available, it may now be possible to perform single crystal neutron scattering measurements in a reflection geometry to beat the ^{157}Gd absorption problem in high quality single crystals with natural Gd abundance [18], and allow for a quantitative investigation of the development of correlations in GGG at low temperatures. This may prove a fruitful endeavor to help shed light on the mysteries of GGG.

We acknowledge the contributions of M. Dion and B. den Hertog to the earlier stage of this project. We thank A. Del Maestro, B. Gaulin, R. Moessner, O. Petrenko, A. Ramirez and P. Schiffer for useful discussions. We thank O. Petrenko for providing neutron data. This work was funded by NSERC of Canada, the Canada Research Chair Program (Tier I) (M.G.), Research Corporation (M.G., M.E.), the Canada foundation for Innovation, the Ontario Innovation Trust, and the Canadian Institute for Advanced research. M.G. acknowledges the U. of Canterbury (UC) for an Erskine Fellowship and the hospitality of the Dept. of Physics and Astronomy at UC where part of this work was completed.

-
- [1] *Frustrated Spin Systems*, ed. H.T. Diep, World Scientific, Singapore (2004).
 - [2] A. P. Ramirez, in *Handbook of Magnetic Materials*, ed.K. H. J. Buschow (Elsevier Science, Amsterdam, 2001), Vol. 13.
 - [3] J.E. Greedan, *J. of Alloys and Compounds* **408-412**, 444 (2006).
 - [4] P. Schiffer *et al.*, *Phys. Rev. Lett.* **74**, 2379 (1995).
 - [5] J. A. Mydosh, *Spin Glasses: An Experimental Introduction*, (Taylor and Francis, London (1993).
 - [6] S.R. Dunsiger *et al.*, *Phys. Rev. Lett.* **85**, 3504 (2000).
 - [7] I.M. Marshall *et al.*, *J. Phys. Condens. Matter* **14**, L157 (2002).
 - [8] P. Bonville *et al.*, *Phys. Rev. Lett.* **92**, 167202 (2004).
 - [9] O.A. Petrenko *et al.*, *Phys. Rev. Lett.* **80**, 4570 (1998).
 - [10] O.A. Petrenko *et al.*, *Physica B* **266**, 41 (1999).
 - [11] W.I. Kinney and W.P. Wolf, *J. Appl. Phys.* **50**, 2115 (1979); W.I. Kinney, Ph.D. thesis, Yale University, 1979.
 - [12] O.A. Petrenko and D. McK. Paul, *Phys. Rev. B* **63**, 024409 (2000).
 - [13] M.J.P. Gingras and B.C. den Hertog, *Can. J. Phys.* **79**, 1339 (2001).

- [14] R.G. Melko and M. J. P. Gingras, *J. Phys.: Condens. Matter* **16**, R1277 (2004).
- [15] P. J. Brown, Magnetic form factors, chapter 4.4.5, in: *International tables for crystallography*, vol. C, pp. 391-399, edited by A. J. C. Wilson (Dordrecht, Holland: D. Reidel Pub. Co., 1983-1993).
- [16] M. Enjalran and M. J. P. Gingras, *Phys. Rev. B* **70**, 174426 (2004) and references therein.
- [17] P. Schiffer *et al.*, *Phys. Rev. Lett.* **73**, 2500 (1994).
- [18] B.D. Gaulin and H. Rønnow, private communications.